Our results show a temporal correlation between tyrosine phosphorylation of actin and cell-shape changes in response to growth conditions and suggest that growth medium induces either the activation of a tyrosine kinase or inhibition of a phosphotyrosine phosphatase that regulates actin tyrosine phosphorylation. This phosphorylation may in turn regulate the alterations in F-actin–containing structures in the cytoskeleton, resulting in cell-shape changes. Changes in the amount of PTP1 affect the kinetics and extent of actin phosphorylation and similarly affect the kinetics and extent of the cell-shape changes and F-actin staining pattern. It is possible that PTP1 does not directly dephosphorylate pTyr-actin and that the effects of PTP1 activity may be propagated through a series of responding proteins. Because the amount of growth-stimulated actin tyrosine phosphorylation in *ptp1* null cells decreases to an amount similar to that seen in wild-type cells, a second PTP may dephosphorylate actin in the absence of PTP1. *Amoeba proteus* actin is phosphorylated in vitro in cell-free extracts in response to Ca^{2+} (the phosphorylated amino acid is unknown) and has been shown to affect actin polymerization in vitro (*15*). Although actin phosphorylation has not been reported in vertebrates, tyrosine phosphorylation of nonactin proteins is essential for conversion of globular (G)-actin to F-actin in B lymphocytes (*16*). The observed changes in *Dictyostelium* may be analogous to cytoskeleton changes in mammalian cells mediated by serum and other extracellular factors or protooncogene activation (*17*).

Note added in proof. Schweiger *et al.* (*18*) also recently showed pTyr-actin in *Dictyostelium*.

REFERENCES AND NOTES

1. S. R. Farmer and L. E. Dike, in *Cell Shape Determinants, Regulatory Role*, W. D. Stein and F. Bronner, Eds. (Academic Press, San Diego, CA, 1989), pp. 173–202; W. Kabsch and J. Vandekerckhove, *Annu. Rev. Biophys. Biomol. Struct.* **21**, 49 (1992).
2. G. Gerisch, *Annu. Rev. Physiol.* **44**, 535 (1982); S. J. McRobbie and P. C. Newell, *Biochem. Biophys. Res. Commun.* **115**, 351 (1983); S. J. McRobbie, *CRC Crit. Rev. Microbiol.* **13**, 335 (1986); P. N. Devreotes and S. H. Zigmond, *Annu. Rev. Cell Biol.* **4**, 649 (1988); J. Condeelis, *Dev. Genet.* **11**, 333 (1990); C. H. Berlot, J. A. Spudich, P. N. Devreotes, *Cell* **43**, 307 (1985); S. Yumura and Y. Fukui, *Nature* **314**, 194 (1985); R. P. Futrelle, J. Traut, W. George McKee, *J. Cell Biol.* **92**, 807 (1982).
3. A. Weeds, *Nature* **296**, 811 (1982); T. D. Pollard and J. A. Cooper, *Annu. Rev. Biochem.* **55**, 987 (1986).
4. A. Shariff and E. J. Luna, *Science* **256**, 245 (1992).
5. P. Howard, B. Sefton, R. A. Firtel, *Cell* **71**, 637 (1992).
6. HL5 contains yeast extract, peptone, glucose, and salts.
7. P. Howard, B. Sefton, R. A. Firtel, unpublished data.
8. M. Mehdy and R. A. Firtel, *Mol. Cell. Biol.* **5**, 705 (1985).
9. Cells were lysed in 0.5% SDS, 1 mM dithiothreitol, and 50 mM tris (pH 8.8) and then diluted with 4 volumes of RIPA buffer without SDS [0.15 M NaCl, 0.01 M $NaPO_4$ (pH 7.2), 1% aprotinin, 1% sodium deoxycholate, 1% NP-40]. Lysates were incubated with antibody for 40 min at 4°C and then with protein A–conjugated Sepharose beads for 40 min. After centrifugation, the sedimental beads were rinsed four times with RIPA buffer.
10. J. I. Garrels and W. Gibson, *Cell* **9**, 793 (1976); C. MacLeod, R. A. Firtel, J. Papkoff, *Dev. Biol.* **76**, 263 (1980); P. Romans and R. A. Firtel, *J. Mol. Biol.* **186**, 337 (1985).
11. M. McKeown and R. A. Firtel, *J. Mol. Biol.* **151**, 593 (1981); *Cold Spring Harbor Symp. Quant. Biol.* **46**, 495 (1982).
12. P. A. Amato, E. R. Unanue, D. L. Taylor, *J. Cell Biol.* **96**, 750 (1983); A. L. Hall, A. Schlein, J. Condeelis, *J. Cell. Biochem.* **37**, 285 (1988).
13. F. T. Marin, *Dev. Biol.* **48**, 110 (1976).
14. J. Franke and R. Kessin, *Proc. Natl. Acad. Sci. U.S.A.* **74**, 2157 (1977).
15. J. Sonobe, S. Takahashi, S. Hatano, K. Kuroda, *J. Biol. Chem.* **261**, 14837 (1986).
16. I. Melamed, G. P. Downey, C. M. Roifman, *Biochem. Biophys. Res. Commun.* **176**, 1424 (1991).
17. V. Ambros, L. B. Chen, M. Buchanan, *Proc. Natl. Acad. Sci. U.S.A.* **72**, 3144 (1975); K. Mellstrom, C.-H. Heldin, B. Westermark, *Exp. Cell Res.* **177**, 347 (1988); K. Burridge, *Cancer Rev.* **4**, 18 (1986); R. G. Watts, M. A. Chrispens, T. H. Howard, *Cytoskeleton* **19**, 159 (1991).
18. A. Schweiger *et al.*, *J. Cell Sci.* **122**, 601 (1992).
19. M. P. Kamps and B. M. Sefton, *Oncogene* **2**, 305 (1988).
20. M. P. Kamps, *Methods Enzymol.* **201**, 21 (1991).

21. Anti-actin was a gift of Dr. Annamma Spudich, Stanford University [P. A. Simpson, J. A. Spudich, P. Parham, *J. Cell Biol.* **99**, 287 (1984)]. We thank members of the laboratories of R. A. Firtel, B. Sefton, and T. Hunter and R. Gomer for helpful suggestions. Supported by U.S. Public Health Service grants to R.A.F. and B.S.

17 August 1992; accepted 16 October 1992

Forward Plasma Membrane Flow in Growing Nerve Processes

Sergey Popov,* Abraham Brown, Mu-ming Poo†

Nerve growth requires addition of new plasma membrane material, which is generally believed to occur at the growth cone. Local incorporation of a fluorescent lipid analog into the plasma membrane of fast-growing *Xenopus* neurites revealed an anterograde bulk membrane flow that correlated with neurite elongation. The rate of membrane flow depended on the position of the labeled membrane segment along the neurite, increasing with distance from the soma. This result suggests that new membrane in growing *Xenopus* neurites is added not at the growth cone but at the cell body and along the neurite.

It is generally accepted that the new plasma membrane material required for nerve growth is added at the tip of the neurite, known as the growth cone (*1*). This view of nerve growth originated mainly from the observation that extracellular particles attached to the neurite surface remain stationary relative to the soma as the neurite elongates (*2*). However, it is possible that some of the particles on the neurite surface were anchored to the neuronal cytoskeleton through transmembrane linkage, and the behavior of the particles reflects the movement of the cytoskeleton rather than that of the plasma membrane (*3*, *4*). Here we show that when fluorescent lipid molecules are locally inserted into the plasma membrane of *Xenopus laevis* neurites, they move forward as the neurite grows; thus, in this system, membrane is added not at the growth cone but at the soma and along the length of neurite.

Cultured *Xenopus* spinal neurons were prepared on laminin-coated glass cover slips (*5*) and were used 3 to 8 hours after plating. At this time, the average rate of neurite extension was 79 ± 19 μm/hour (SEM, n = 49) at room temperature (20° to 22°C). In the first set of experiments, neurons with relatively long neurites (~400 μm) were selected, and the fluorescent lipid analog 1,1′-didodecyl-3,3,3′,3′-tetramethylindocarbocyanide perchlorate ($DiIC_{12}$) was incorporated into a segment of neurite membrane close to the growth cone (at a distance of 60 to 80 μm from the neurite tip) by a local perfusion method (*6*). Analysis of the differential interference contrast (DIC) and fluorescence images of the neurite at two different times after local perfusion of the fluorescent lipid (Fig. 1) revealed that the incorporated lipid molecules rapidly spread along the membrane. The profiles of the fluorescence distribution during the first 5 min after perfusion were measured with a digital imaging method (*7*), and the positions of the center of the profiles were determined (*8*). For actively growing neurites (Fig. 1, A through C), we observed a shift of the center of the profile in the anterograde direction. In 17 cases in which elongation of the neurites was observed, the center of the fluorescence profile moved forward at a rate of 2.1 ± 0.2 μm/min (SEM) as the neurite elongated at a rate of

Department of Biological Sciences, Columbia University, New York, NY 10027.

*On leave from the Institute of Electrochemistry, Academy of Sciences, Moscow, Russia.
†To whom correspondence should be addressed.

2.3 ± 0.2 μm/min. When the rate of anterograde movement of the profile was compared to the rate of neurite elongation for each neurite, the average ratio was 0.91 ± 0.06. In contrast, in 11 other cases where no detectable neurite elongation (<1 μm) occurred over the period of observation (~5 min) (Fig. 1D), the center of the profile remained stationary with an average displacement of 0.03 ± 0.02 μm/min. Thus, for growing neurites, the plasma membrane behind the growth cone flows forward at a rate close to that of neurite elongation, indicating no substantial membrane addition at the growth cone.

Theoretical analysis of fluorescence profiles at various times after lipid incorporation (9) showed that the $DiIC_{12}$ molecules diffused along the neurite with a diffusion coefficient of $(2.0 \pm 0.1) \times 10^{-8}$ cm^2/s (SEM, $n = 24$). This value is consistent with that expected for lateral diffusion of lipids in the plasma membrane (*10*), suggesting that most of the fluorescent lipid molecules are properly incorporated into the plasmalemma. The plasmalemma localization of the incorporated lipids was also indicated by the ring staining of the soma and the absence of cytosolic staining during the first 10 min after perfusion of the soma, as revealed by confocal fluorescence microscopy. This result supports previous findings with similar DiI molecules (*11*). The absence of significant lipid internalization during the brief period of these experiments was further indicated by the uniform fluorescence staining along the neurite. Punctate fluorescence that reflects lipid internalization was not detected during the first 10 min after perfusion.

To determine in which region of the neuron the new membrane is inserted, we measured the rate of membrane flow at the middle segment of the neurite (Fig. 2A) and near the soma (Fig. 2B). In a total of 23 experiments, we consistently observed an anterograde shift in the center of the fluorescence profile, indicative of anterograde membrane flow. The rate of flow depended on the position of the labeled segment along the neurite, increasing with distance from the soma. To normalize the data, we plotted the rate of membrane flow relative to the rate of neurite elongation against the relative distance of the labeled segment from the soma (Fig. 2C), including data obtained near the growth cone. The nonzero slope of the line that best fits the data can be explained by uniform insertion of membrane material along the length of neurite or by a decrease in neurite diameter with time without membrane addition. Both of these effects will result in an apparent membrane flow whose rate increases with distance from the soma.

Estimation of the contribution of neurite diameter change to the observed membrane flow required a convenient method of determining the extent of membrane flow over a defined segment of neurite. This problem was resolved when we found that yolk granules that were attached to the neurite surface could serve as convenient markers of the membrane. These yolk granules, which originated from broken cells during plating of the culture, remained extracellular after attaching to the neurite, as shown by their staining with the membrane-impermeant dyes Trypan blue and Lucifer yellow. In total, 102 granules were traced in 49 elongating neurites. We consistently observed anterograde movements of the granules along the neurite (Fig. 3, A and B). The rate of granule movement depended on the position of the granules along the neurite, increasing with distance between the granule and the soma. When

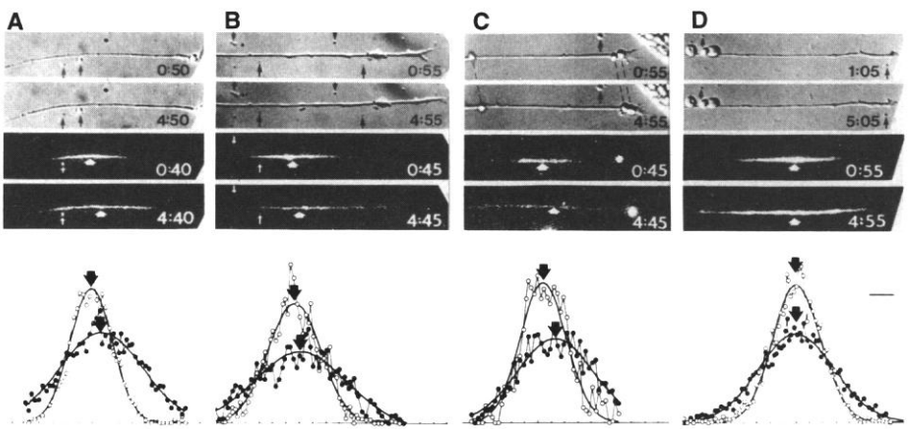

Fig. 1. Membrane flow in *Xenopus* neurites revealed by local incorporation of the fluorescent lipid analog $DiIC_{12}$. (**A**, **B**, **C**, and **D**) DIC images, fluorescence images, and profiles of fluorescence intensities along four neurites at two different times (marked as min:s) after local perfusion of the neurite with a solution containing $DiIC_{12}$ (10 μg/ml). Small black and white arrows mark fixed reference points in the culture, and large white arrows mark the center of the fluorescence distribution. Dashed black lines in the DIC images in (C) indicate the anterograde movement of yolk granules attached to the surface of the neurite. Data points (circles) on the graph are the relative intensities of the fluorescence along the neurite measured by a digital imaging method at two different times corresponding to the times shown in the fluorescence images. The centers of the fluorescence profiles are marked by the large black arrows. Solid lines represent Gaussian profiles that best fit the data. The anterograde shift in the center of diffusion curve for elongating neurites was 6.8 μm (A), 4.5 μm (B), and 8.9 μm (C). For nonelongating neurite (D), the shift was −0.3 μm. Bar = 20 μm.

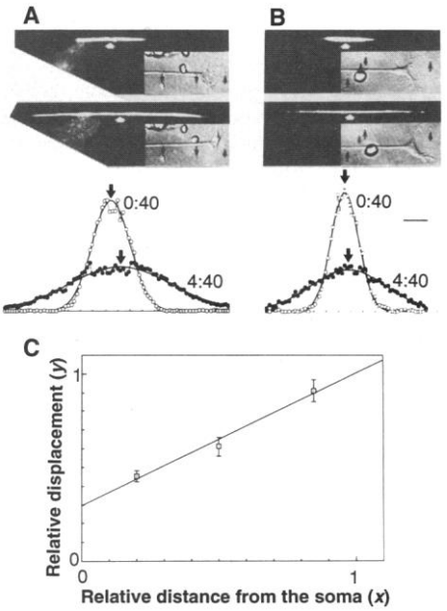

Fig. 2. Membrane flow in *Xenopus* neurites at (**A**) the middle of the neurite and (**B**) near the soma. Fluorescence images of the labeled segments of neurites, corresponding DIC images of the growth cone of the same neurite, and profiles of fluorescence intensities along two neurites at two different times (marked as min:s). The arrows are as in Fig. 1. The labeled segment in (A) was in the middle of the neurite, about 200 μm from both the soma and the growth cone; the labeled segment in (B) was in the proximal portion of the neurite, about 80 μm from the soma. The anterograde shift in the center of fluorescence profile curve was 7.3 μm (A) and 3.0 μm (B). Bar = 20 μm. (**C**) The distance of the labeled segment from the soma (ℓ) was normalized to the length of the neurite (L) to obtain the relative distance ($x = \ell/L$). The shift in the peak of the profile during the time of the experiment ($\Delta\ell$) was normalized against the extension of the neurite (ΔL) over the same duration to yield the relative displacement ($y = \Delta\ell/\Delta L$). Data are the mean of y values for the points close to the soma ($x = 0.2$, $n = 12$), in the middle of neurite ($x = 0.5$, $n = 11$), and near the growth cone ($x = 0.85$, $n = 17$). The error bars refer to SEM. The solid line represents the best linear fit of all data, given by the expression $y = 0.30 + 0.69x$.

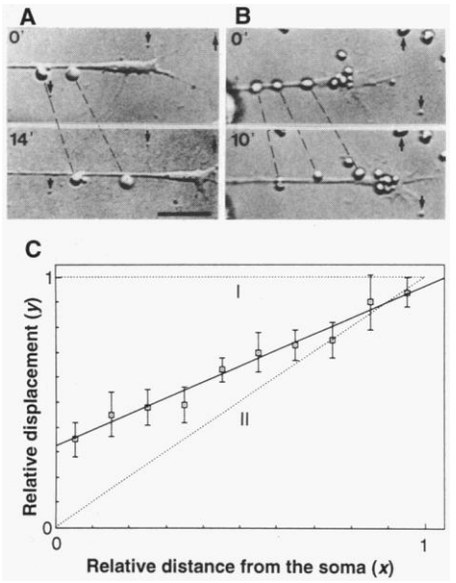

Fig. 3. Anterograde movements of surface-bound yolk granules along elongating neurites. (**A** and **B**) DIC images of two neurites at two different times (marked in minutes) during neurite elongation. Arrows mark fixed reference points in the substratum. Dashed lines connect the initial and final positions of the same granule. Note the higher rate of movement for granules closer to the growth cone (on the right end) and the increasing separation between granules with time. Bar = 20 μm. (**C**) Rate of granule movements at different distances from the soma. The distance of the granules from the soma and the rate of granule translocation were normalized as in Fig. 2C. The x values were divided into ten bins, and the data are the mean of the y values within each bin. The error bars refer to SEM, and the number of granules examined for each bin ranged from 6 to 20 (total 102). The solid line represents the best linear fit of all data, given by the expression $y = 0.32 + 0.64x$. The dashed lines I and II represent predictions of granule movements by two different models of membrane addition during neurite growth. Model I, plasma membrane flow from the soma to the neurite accounts for all the new membrane during neurite elongation; model II, the new membrane is uniformly added along the length of neurite, with no membrane flow from the soma.

the data were normalized, we found that the granules at the distal segment of neurite (x = 0.8 to 1.0), in the middle of neurite (x = 0.4 to 0.6), and near the soma (x = 0.0 to 0.2) all moved at a rate close to that of membrane flow at the corresponding regions. Because the yolk granules move at the same rate as the plasma membrane, a set of yolk granules can be used to indicate the extent of membrane flow within defined segments of the neurite. The change in the neurite diameter during elongation was measured, with high-resolution DIC optics, between two adjacent yolk granules as their separation increased over a period of 45 min. For nine pairs of granules examined, the diameter of the neurite showed an average reduction of 38 ± 10% (SEM), whereas the distances between the granules showed an average increase of 93 ± 18%, which is about 2.4 times the expected increase for extension without addition of new membrane (*12*). Thus, the increased separation of adjacent yolk granules with time cannot be accounted for simply by a decrease in neurite diameter. A substantial amount of new membrane must have been incorporated into the plasmalemma along the length of the neurite. Furthermore, substantial membrane flow from the cell body to the neurite must have occurred because the average rate of granule movement near the soma (x = 0.0 to 0.1) was significantly higher than zero (y = 0.35 ± 0.07, n = 11) (Fig. 3C). In fact, the best-fit curves for both data sets (Fig. 2C and Fig. 3C) cross the y-axis at a point close to 0.3, which also indicates that a substantial fraction of the neuritic membrane was derived from the soma.

This study provides evidence that elongation of nerve processes may depend on an anterograde bulk membrane flow along the neurite. In these fast-growing *Xenopus* neurons in culture, new plasma membrane material appears to be inserted at the soma and along the neurite rather than at the growth cone. Microtubules also translocate in an anterograde direction along these *Xenopus* neurites (*3*, *13*). The rate of this translocation and its dependence on the position along the neurite were similar to those reported here for membrane flow. Whether the membrane flow and microtubule translocation are coupled and what drives the membrane flow are questions that remain to be investigated.

REFERENCES AND NOTES

1. B. Alberts *et al.*, *Molecular Biology of the Cell* (Garland, New York, ed. 2, 1989).
2. D. Bray, *Proc. Natl. Acad. Sci. U.S.A.* **65**, 905 (1970); *J. Cell Biol.* **56**, 702 (1973).
3. S. Okabe and N. Hirokawa, *J. Cell Biol.* 117, 105 (1992).
4. P. Forscher, C. H. Lin, C. Thompson, *Nature* **357**, 515 (1992); P. Forscher and S. J. Smith, *J. Cell Biol.* **107**, 1505 (1988); M. Edidin, S. C. Kuo, M. P. Sheetz, *Science* **254**, 1379 (1991).
5. The procedure for preparing *Xenopus* nerve-muscle cultures has been reported [N. C. Spitzer and H. E. Lamborghini, *Proc. Natl. Acad. Sci. U.S.A.* **73**, 1641 (1976); M. J. Anderson, M. W. Cohen, E. Zorychta, *J. Physiol. London* **268**, 731 (1977); N. Tabti and M.-m. Poo, in *Culturing Nerve Cells*, G. Banker and K. Goslin, Eds. (MIT Press, Cambridge, MA, 1991)]. Briefly, the neural tube and the associated myotomal tissue of 1-day-old *Xenopus* embryos [stage 20 to 22, P. D. Nieuwkoop and J. Faber, *Normal Table of* Xenopus laevis (North-Holland, Amsterdam, ed. 2, 1967)] were dissociated in Ca^{2+}- and Mg^{2+}-free saline supplemented with EDTA. The cells were plated on glass cover slips precoated with laminin (3 to 4 μg/cm²; Sigma). The culture medium consisted of (v/v) 50% Leibovitz L-15 medium (Sigma) and 50% Ringer solution (115 mM NaCl, 2 mM $CaCl_2$, 2.5 mM KCl, 10 mM Hepes; adjusted to pH 7.8).
6. Local perfusion of the neurite was performed with two micropipettes located 5 to 10 μm away from the neurite surface. The first pipette [inner diameter (ID) 6 to 9 μm] was filled with phosphate-buffered saline (PBS) containing $DiIC_{12}$ (10 μg/ml). A small hydrostatic pressure (2 to 5 mm of H_2O) applied to the pipette resulted in a constant outflow of the intrapipette solution. The second pipette (ID 12 to 14 μm) was used for removal of DiC_{12} solution by applying suction. The pipettes were withdrawn from the neurite 30 s after the onset of surface labeling.
7. The fluorescence images were recorded with an inverted microscope (Axiovert, Zeiss) equipped with a ×40 oil immersion lens (numerical aperture 0.9) and rhodamine filter set. The images were collected by a cooled charge-coupled device (CCD) camera (Photonics, model Star I), stored with an optical disk recorder (Panasonic Model TQ-2026 F), and analyzed with a digital image processor (Imaging Technology, Model 151). Typically, we obtained the distribution of fluorescence intensity by measuring the total intensity within rectangular sampling areas (1.08 μm²) along the length of neurite. The sampling was started 60 to 80 μm proximal to the center of a labeled segment with regular spacing of 1.6 to 2.3 μm along the neurite. The background fluorescence, measured at cell-free areas 5 to 10 μm away from the corresponding spots along the neurite, was subtracted from the fluorescence at the neurite.
8. Two methods were used to determine the position of the center (x_{center}) of the fluorescence distribution. First, we used a "center of mass" calculation that was based on the following formula: $x_{center} = \Sigma I_i x_i / \Sigma I_i$, where I_i is the fluorescence intensity at a distance x_i from the first sampling spot after background subtraction. Second, we used the Gaussian profile that describes one-dimensional diffusion from a point source:

$$I(x,t) = (A/c^{1/2}) \exp[-(x - x_{center})^2/4c]$$

where A and c are constants. The data points I_i for a given time t were least squares fitted to the Gaussian profile to determine x_{center}. The shift of x_{center}, or Δx_{center}, indicates the bulk flow of the membrane. The two methods of estimating Δx_{center} yielded essentially the same results, with differences of less than 1 μm in all 28 cases.
9. We estimated the diffusion coefficient (D) of $DiIC_{12}$ in the neuronal plasma membrane from the fluorescence profiles obtained 4.0 to 5.2 min after the start of labeling using the formula $D = c/t$, where we determined c by fitting experimental data to the equation $I(x,t)$ (*8*) at a corresponding time t. Because this time was much longer than the duration of the labeling (<30 s), the initial condition of diffusion was assumed to be a point source [S. V. Popov and M.-m. Poo, *J. Neurosci.* **12**, 77 (1992)].
10. D. W. Tank, E.-S. Wu, W. W. Webb, *J. Cell Biol.* **92**, 207 (1982).
11. J. Lee, M. Gustafsson, K.-E. Magnusson, K. Jacobson, *Science* **247**, 1229 (1990).
12. If a neurite has a cylindrical shape, the total surface area of a segment with length ℓ and radius r will be $2\pi r\ell$. Thus the ratio (ℓ_2/ℓ_1) is equal to the ratio (r_1/r_2) at two different times when no new membrane is added.
13. S. S. Reinsch, T. Mitchison, M. Kirschner, *J. Cell Biol.* **115**, 365 (1991); E. Tanaka and M. Kirschner, *ibid.*, p. 345.

14. This work was supported by grants from NIH (NS 22764), NSF (BNS 12398), and the Office of Naval Research (N00014-90-J1865).

10 September 1992; accepted 19 November 1992